Polymer Chemistry

ROYAL SOCIETY OF CHEMISTRY

PAPER

View Article Online
View Journal | View Issue

Cite this: *Polym. Chem.*, 2022, **13**, 5861

Synthesis of crystallizable poly(behenyl methacrylate)-based block and statistical copolymers and their performance as wax crystal modifiers†

Isabella R. Dorsman,[a] Derek H. H. Chan,[a] Victoria J. Cunningham,[b] Steven L. Brown,[b] Clive N. Williams,[b] Spyridon Varlas *[a] and Steven P. Armes *[a]

Two series of behenyl methacrylate-based diblock and statistical copolymers have been prepared by reversible addition–fragmentation chain transfer (RAFT) solution polymerization in *n*-dodecane and evaluated as additives for the crystal habit modification of a model wax (*n*-octacosane). DSC studies indicated that each statistical copolymer exhibited a significantly lower crystallization temperature (T_c) and melting temperature (T_m) for the semi-crystalline behenyl methacrylate component than the corresponding diblock copolymer of almost identical overall composition. Temperature-dependent turbidimetry studies were conducted for each copolymer using a series of solutions of 5.0% w/w *n*-octacosane dissolved in *n*-dodecane to determine T_{cool}, which is the temperature at which zero transmittance is first observed owing to wax crystallization. At a constant molar copolymer concentration of 0.26 mM, each of the eight copolymers produced a reduction in T_{cool} of approximately 3–5 °C. Scanning electron microscopy (SEM) studies confirmed that the presence of such copolymers led to a reduction in the overall size and/or a higher crystal aspect ratio. The diblock and statistical copolymers were similar in their performance as potential wax crystal modifiers. However, the statistical copolymers were easier to prepare and did not suffer from any homopolymer contamination. Moreover, optical microscopy and SEM studies revealed that needle-like crystals were formed instead of platelets when employing behenyl methacrylate-rich statistical copolymers.

Received 5th August 2022,
Accepted 26th September 2022

DOI: 10.1039/d2py01023b

rsc.li/polymers

Introduction

The formation of insoluble paraffinic wax crystals in oil at sub-ambient temperature is a long-standing problem that causes pipeline blockages in cold climates.[1,2] This is an important issue for both crude oil transportation and the delivery of diesel fuel to automotive engines.[3–6] The onset temperature at which these *n*-paraffins exceed their solubility limit and precipitate in the form of wax crystals is often denoted as the 'wax appearance temperature' (WAT) or cloud point temperature.[6,7] Such deposits consist of lamellar crystals that form random, interlocking structures containing occluded crude oil.[8] These crystals form a 3D network with as little as 2% w/w solid wax required for gelation.[9,10] Below the WAT, the temperature at which the oil no longer flows under static conditions is known as the pour-point temperature (PPT).[7,11]

In principle, the precipitation of wax crystals can be suppressed by the addition of suitable oil-soluble copolymers, which are known as wax inhibitors (WIs) or pour-point depressants (PPDs), or more broadly as wax crystal modifiers.[6,12] A wide range of copolymers have been evaluated in this context. These include polyethylene-polybutene[8,13–15] or polyethylene-poly(ethylene-*stat*-propylene) diblock and statistical copolymers,[16,17] poly(ethylene-*stat*-vinyl acetate) (EVA)[18–21] or (meth)acrylic[22,23] statistical copolymers and maleic anhydride-based alternating or statistical copolymers.[4,5,24] In each case, one comonomer is designed to interact with the paraffinic wax, while the other comonomer remains solvated and hence confers steric stabilization. Ideally, the critical temperature at which wax crystals are formed is lowered below the relevant working temperature for the oil, so that precipitation is avoided. Alternatively, the crystallization behavior is modified such that the size and shape of the wax crystals do not lead to pipeline blockages. Most studies report a reduction in crystal size in the presence of wax

[a]*Department of Chemistry, University of Sheffield, Dainton Building, Brook Hill, Sheffield S3 7HF, UK. E-mail: s.varlas@sheffield.ac.uk, s.p.armes@sheffield.ac.uk*
[b]*Scott Bader Company Ltd, Wollaston, Wellingborough NN29 7RL, UK*

†Electronic supplementary information (ESI) available: Materials and methods, synthesis protocols, supplementary ^{1}H NMR and UV-vis spectra and SEC curves. See DOI: https://doi.org/10.1039/d2py01023b

inhibitors,[19,25–29] and thus a higher critical gelation concentration (CGC).

Although some studies report no significant change in the WAT in the presence of wax inhibitors,[5,30–32] the addition of such modifiers typically lowers the WAT.[25,33–35] Sjöblom *et al.* used differential scanning calorimetry (DSC) to study a 5% w/w macrocrystalline wax in toluene at a PPD concentration of 1000 ppm and reported a WAT reduction from around 20 °C in the absence of any PPD to 15–19 °C in the presence of five different PPDs.[25] This was attributed to a change in the solubility equilibrium as a result of the formation of solute complexes.[36] A change in crystal morphology was also reported in the same study. Optical microscopy studies indicated that the wax crystals formed in the absence of PPDs exhibited a mixed morphology comprising needles and plates, whereas those formed in the presence of the most effective PPD (a commercial carboxylate-based polymer) possessed a smaller, more compact structure.

In 2015, Binks *et al.* conducted a series of experiments using three model waxes (*n*-eicosane, *n*-tetracosane or *n*-hexatriacontane, *i.e.* $C_{20}H_{42}$, $C_{24}H_{50}$ or $C_{36}H_{74}$).[37] Assuming a thermodynamically ideal solution, the temperature dependence for wax solubility was predicted for *n*-heptane and toluene, which served as model non-polar aliphatic and aromatic solvents respectively. For a given wax concentration, the PPT corresponds to that at which a critical volume fraction of wax crystals has precipitated. Close to this temperature, the wax crystals typically comprise irregular platelets that form a 3D network. Addition of a suitable PPD copolymer typically reduced the size and axial ratio (thickness, *h*/diameter, *d*) of the wax crystals, which in turn increased the critical volume fraction of wax crystals required to form a 3D network (and hence block a pipeline). Moreover, PPD performance was correlated with the difference between the wax and the polymer solubility boundary temperatures for four different copolymers. More specifically, the reduction in PPT for formulations containing 20% wax by mass proved to be most effective when the critical solubility temperature of the PPD copolymer in a given solvent was approximately 15 °C below that of the target wax–solvent system. In principle, this empirical approach provides a useful method for the rapid identification of next-generation PPD copolymers.

Prior research suggests that poly(*n*-alkyl methacrylates) possessing pendant *n*-alkyl groups comprising 20–30 carbon atoms can serve as potential wax crystal inhibitors.[30,37] A recent review article by Chi *et al.* on controlling paraffin deposition in production lines noted that effective wax crystal modifiers typically contained paraffin-like crystalline segments.[6] Such PPD polymers can co-crystallize with and hence influence the formation and structure of wax crystal networks.

Given this encouraging precedent, we decided to evaluate the performance of a range of model copolymers based on behenyl methacrylate (BeMA or Be) for wax crystal modification. Accordingly, two series of well-defined diblock and statistical copolymers were prepared, employing BeMA as the crystallizable component and lauryl methacrylate (LMA or L) as the oil-soluble component (Scheme 1). All copolymers were prepared *via* reversible addition–fragmentation chain transfer (RAFT) solution polymerization to ensure that they possessed relatively narrow molecular weight distributions. For wax crystal modification studies, *n*-octacosane ($C_{28}H_{58}$) was employed as a model wax and the non-polar solvent was *n*-dodecane.

Results and discussion

A $PLMA_{98}$ homopolymer was prepared *via* RAFT solution polymerization of LMA in toluene at 70 °C using PETTC as the chain transfer agent (CTA) (Scheme S2†). This polymerization

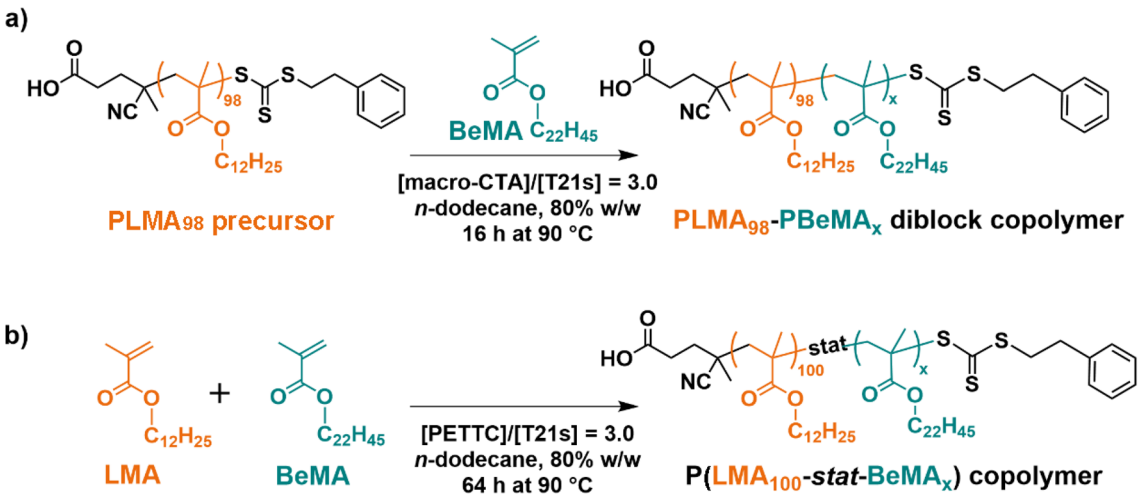

Scheme 1 Synthesis of (a) poly(lauryl methacrylate)$_{98}$-poly(behenyl methacrylate)$_x$ ($PLMA_{98}$-$PBeMA_x$) diblock copolymers (x = 10–60), and (b) poly(lauryl methacrylate$_{100}$-*stat*-behenyl methacrylate$_x$) (P(LMA_{100}-*stat*-$BeMA_x$)) statistical copolymers (x = 10–60) *via* RAFT solution polymerization at 80% w/w solids in *n*-dodecane at 90 °C.

was quenched at 57% conversion to produce a $PLMA_{98}$ precursor with a mean DP of 98, as indicated by end-group analysis using ^{1}H NMR spectroscopy (Fig. S3†). Terminating the RAFT polymerization well below full conversion avoids monomer-starved conditions and hence aids retention of the trithiocarbonate end-groups.[38,39] This is usually considered desirable for ensuring high blocking efficiencies for the subsequent synthesis of poly(lauryl methacrylate)$_{98}$-poly(behenyl methacrylate)$_x$ ($PLMA_{98}$-$PBeMA_x$) diblock copolymers. Analysis by THF SEC using a series of poly(methyl methacrylate) calibration standards indicated a number-average molecular weight (M_n) of 18.0 kg mol^{-1} and a relatively narrow molecular weight distribution ($Đ$ = 1.20).

A series of four $PLMA_{98}$-$PBeMA_x$ (or L_{98}-*b*-Be_x) diblock copolymers and four P(LMA_{100}-*stat*-$BeMA_x$) (or L_{100}-*stat*-Be_x) statistical copolymers, where x = 10, 20, 40 and 60, were subsequently prepared *via* RAFT solution polymerization in *n*-dodecane at 90 °C (Scheme 1). Given its relatively high molar mass (395 g mol^{-1}), BeMA monomer has a relatively low molar concentration for a given mass concentration compared to other common methacrylic monomers, *e.g.* methyl methacrylate (100 g mol^{-1}). Thus, syntheses were conducted at 80% w/w solids to ensure that a high BeMA conversion could be obtained. All copolymerizations were conducted using an organic peroxide T21s initiator using a [$PLMA_{98}$]/[T21s] or [PETTC]/[T21s] molar ratio of 3.0.

After 16 h at 90 °C, at least 98% BeMA conversion was achieved for all four $PLMA_{98}$-$PBeMA_x$ diblock copolymers, as determined by ^{1}H NMR spectroscopy (Fig. 1 and Table 1). THF SEC analysis of the purified copolymers indicated M_n values ranging between 21.4 kg mol^{-1} and 33.2 kg mol^{-1} and relatively narrow molecular weight distributions ($Đ \leq 1.25$), which suggests good RAFT control (Table 1). Comparison with the SEC trace obtained for the $PLMA_{98}$ precursor confirmed relatively high blocking efficiencies, although a low molecular weight shoulder is evident when targeting PBeMA DPs of 40 or 60 (Fig. 2a). Reaction times were increased to 64 h for the synthesis of the P(LMA_{100}-*stat*-$BeMA_x$) statistical copolymers to ensure at least 99% comonomer conversion (Table 1). THF SEC analysis of the as-synthesized copolymers indicated copolymer M_n values of 24.4–39.6 kg mol^{-1} and relatively low dispersities (Fig. 2b).

Prior to their examination as wax crystal modifiers, all copolymers were purified to remove residual BeMA monomer by precipitation (twice) into excess ethanol at 35 °C. ^{1}H NMR spectroscopy confirmed the disappearance of the vinyl signals

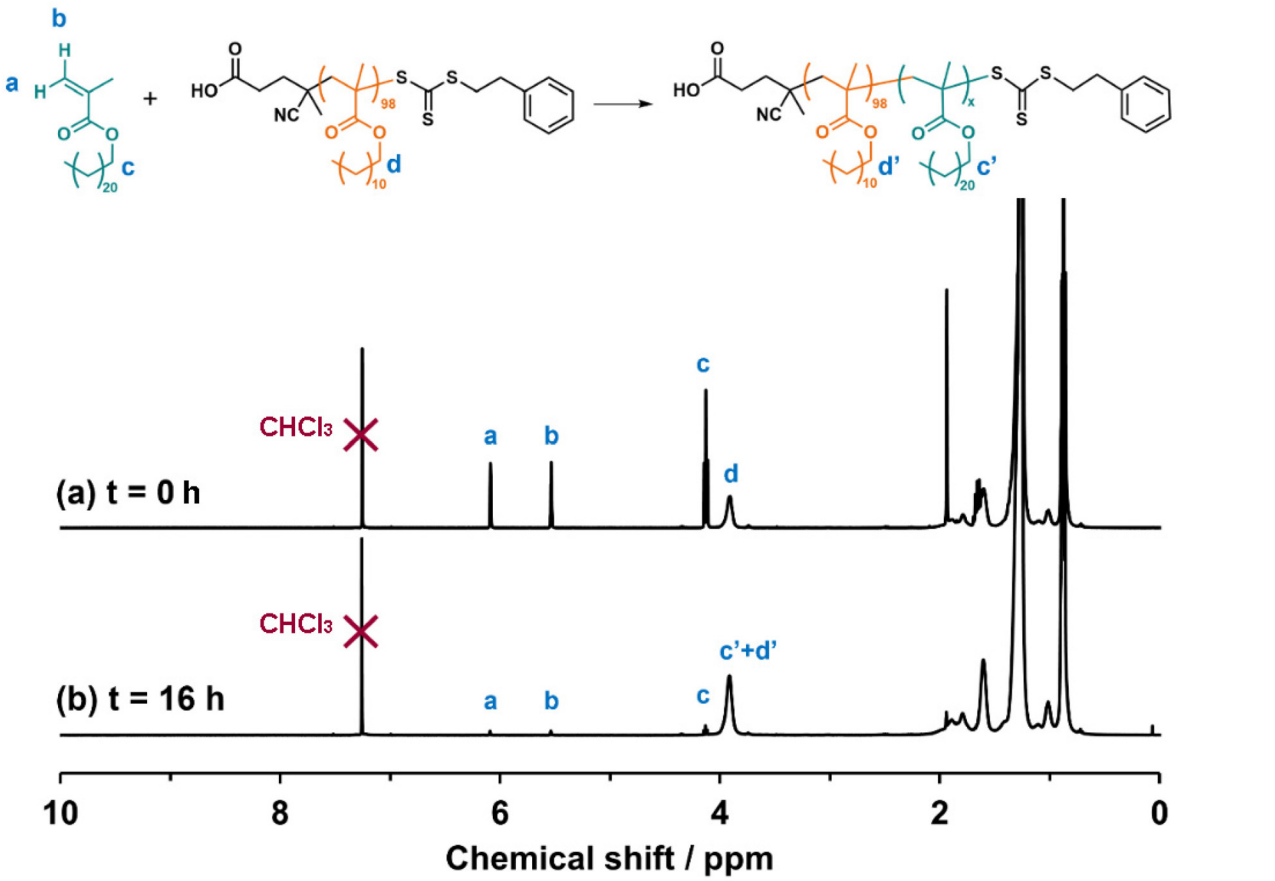

Fig. 1 Partially assigned ^{1}H NMR spectra ($CDCl_3$) recorded for (a) the reaction mixture at zero time (t = 0 h) containing a $PLMA_{98}$ precursor and BeMA monomer, and (b) the same reaction mixture after polymerization for 16 h to form a $PLMA_{98}$-$PBeMA_{60}$ diblock copolymer.

Table 1 Summary of (co)polymer compositions, (co)monomer conversions, SEC molecular weights and dispersities, and T_c and T_m values determined by DSC for the two series of BeMA-based diblock and statistical copolymers after their purification by precipitation into excess ethanol

(Co)polymer composition	(Co)monomer conversion[a]/%	M_n[b]/kg mol^{-1}	$Đ$[b]	T_c[c]/°C	T_m[c]/°C
L_{98}	—	18.0	1.20	−44.3	−36.8
Be_{37}	—	12.5	1.14	48.3	60.0
L_{98}-*b*-Be_{10}	99	21.1	1.18	28.7	45.1
L_{98}-*b*-Be_{20}	>99	24.3	1.19	39.3	50.5
L_{98}-*b*-Be_{40}	99	30.4	1.20	41.7	53.5
L_{98}-*b*-Be_{60}	98	39.4	1.17	43.9	54.4
L_{100}-*stat*-Be_{10}	>99	26.1	1.15	−34.6	−27.1
L_{100}-*stat*-Be_{20}	>99	28.1	1.18	−16.8	−1.4
L_{100}-*stat*-Be_{40}	99	32.1	1.21	0.5	16.9
L_{100}-*stat*-Be_{60}	99	39.1	1.23	11.0	26.1

[a] Determined by ^{1}H NMR spectroscopy. [b] Determined by THF SEC and expressed relative to a series of poly(methyl methacrylate) calibration standards. [c] Determined by DSC (all copolymers were subjected to two thermal cycles to remove any hysteresis effects).

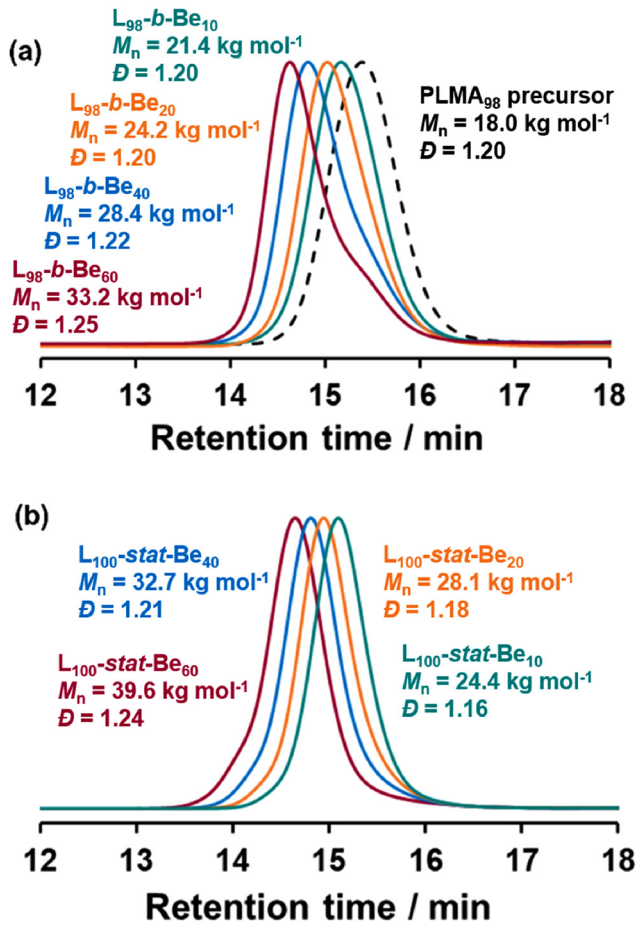

Fig. 2 THF SEC traces recorded for (a) a $PLMA_{98}$ precursor and the corresponding $PLMA_{98}$-$PBeMA_x$ diblock copolymers, and (b) P(LMA_{100}-*stat*-$BeMA_x$) statistical copolymers. [N.B. All copolymers were analysed prior to their purification by precipitation into excess ethanol].

between 5.5 and 6.1 ppm, indicating the complete removal of unreacted monomer(s). Comparison of the SEC traces recorded for $PLMA_{98}$-$PBeMA_x$ diblock copolymers before (Fig. 2) and after (Table 1) such purification indicated only a modest difference between the initial and final M_n in each case, along with a marginally narrower molecular weight distribution (Fig. S5†).

To aid the assessment of copolymer structure on wax crystal modification performance, a $PBeMA_{37}$ homopolymer previously prepared by Derry *et al.*[40] was also examined as a control. Differential scanning calorimetry (DSC) was used to determine the crystallization temperature (T_c) and melting temperature (T_m) for the semi-crystalline PBeMA chains in the $PBeMA_{37}$ homopolymer and the eight diblock and statistical copolymers.[41,42] A summary of the THF SEC and DSC data obtained for all eight purified copolymers and also for the reference $PLMA_{98}$ and $PBeMA_{37}$ homopolymers is provided in Table 1.

It is well-known that both PBeMA and PLMA are semi-crystalline polymers. T_m values of 60.0 °C and −36.8 °C were measured for $PBeMA_{37}$ and $PLMA_{98}$, respectively. These compare well to the literature values.[40,43] Notably, PLMA exhibits relatively subtle melting and crystallization transitions compared to PBeMA because the former homopolymer is much less crystalline (Fig. 3). According to the literature, PLMA exhibits a T_g of −65 °C.[44,45] It is likely that this transition is obscured by the broad T_m peak for the $PLMA_{98}$ homopolymer shown in Fig. 3.[43]

The four $PLMA_{98}$-$PBeMA_x$ diblock copolymers exhibit well-defined peaks for crystallization and melting, with both T_c and T_m lying above ambient temperature (25 °C). Both transition temperatures increase as the DP of the PBeMA block is raised and approach the T_c and T_m values observed for the pure

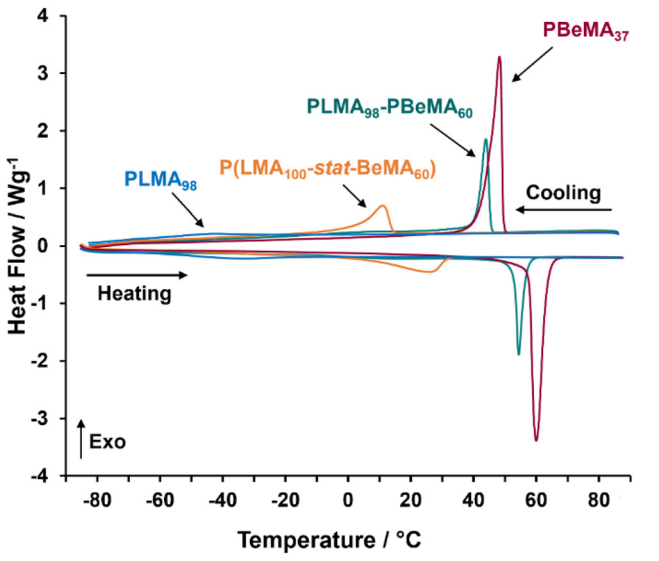

Fig. 3 DSC traces conducted at a cooling/heating rate of 10 °C min^{-1} showing T_c values (exothermic) and T_m values (endothermic) for $PLMA_{98}$-$PBeMA_{60}$ diblock and P(LMA_{100}-*stat*-$BeMA_{60}$) statistical copolymers, as well as the $PBeMA_{37}$ and $PLMA_{98}$ reference homopolymers.

PBeMA$_{37}$ homopolymer (T_c = 48.3 °C; T_m = 60.0 °C). Such thermal transitions are attributed to crystallization of the PBeMA blocks. However, no separate T_c and T_m values for the less crystalline PLMA block was observed for these diblock copolymers when using a heating/cooling rate of 10 °C min^{-1}. The four P(LMA$_{100}$-*stat*-BeMA$_x$) statistical copolymers displayed broader, more subtle thermal transitions, with most T_c and T_m values occurring below 25 °C. In this case, crystallization arises from self-organization of the pendent behenyl groups randomly located along the methacrylic backbone. This difference is also reflected in the differing physical appearance of these copolymers. At ambient temperature, the four statistical copolymers form viscous fluids, whereas the four diblock copolymers are solids.

n-Octacosane ($C_{28}H_{58}$) was selected as a single-component model wax and was employed as a 5.0% w/w solution in *n*-dodecane. This concentration is at the lower end of the typical wax content in crude oils (5–30% w/w)[12], but such conditions produced sufficient wax crystals for characterization by optical and scanning electron microscopy (SEM). Moreover, Ashbaugh *et al.*[19] and Kurniawan *et al.*[46] used comparable wax concentrations in their studies. Macrocrystalline paraffin wax comprises mainly low molecular weight *n*-alkanes (C_{16}–C_{40}) and generally crystallizes in the form of either needles or platelets.[12] Indeed, wax crystal platelets are observed on cooling a 5.0% w/w solution of *n*-octacosane dissolved in *n*-dodecane in the present study (Fig. 4a and b). Prior literature reports suggested that an initial copolymer concentration of 1.0% w/w should be selected for initial experiments.[37,47] For PLMA$_{98}$–PBeMA$_{10}$, this is equivalent to a copolymer concentration of 0.26 mM. This molar concentration was held constant for all copolymers throughout our investigation to ensure that the same number of copolymer chains were present in each experiment when varying the copolymer composition (*i.e.* 2.1 × 10^{17} chains per gram of solution).

Effective wax crystal modifiers act by lowering the critical WAT required for the onset of crystallization of paraffin wax.[6] To examine how the present copolymers influence the WAT of a model wax, turbidimetry measurements were conducted using 5.0% w/w *n*-octacosane dissolved in *n*-dodecane. Initial experiments were performed at a copolymer concentration of 0.26 mM. Thermal cycles from 50 °C to 0 °C to 50 °C were conducted three times at a cooling/heating rate of 1.0 °C min^{-1}. Representative data obtained for one such thermal cycle performed in the absence of any copolymer are presented in Fig. 4c, along with digital photographs indicating the physical appearance of the *n*-octacosane/*n*-dodecane mixture recorded at 50 °C and 0 °C, respectively. Tang and co-workers employed a similar light transmittance method to evaluate WATs for model paraffin waxes in *n*-decane in the presence and absence of wax crystal inhibitors.[35]

The *n*-octacosane/*n*-dodecane mixture forms a highly transparent solution at 50 °C (100% transmittance), but becomes opaque (0% transmittance) on cooling owing to wax crystallization. A WAT is observed at around 23 °C, below which a sharp reduction in transmittance is observed. T_{cool} is taken to be the

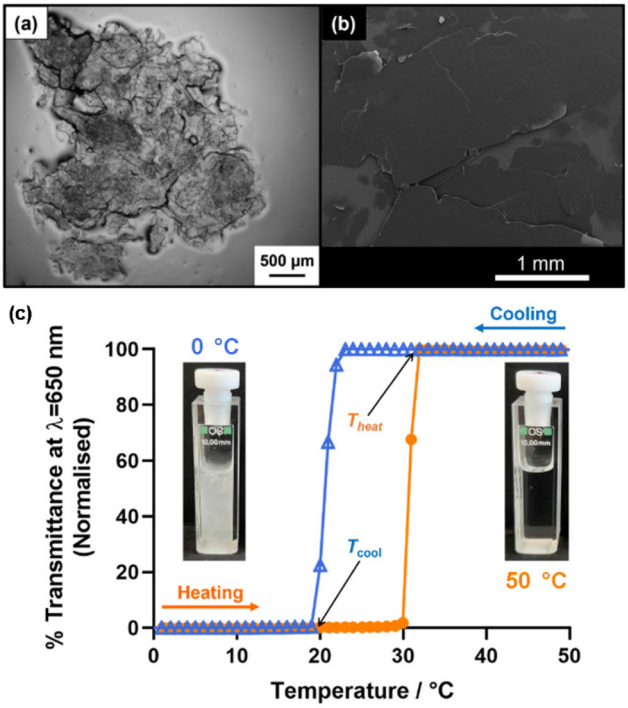

Fig. 4 Digital images recorded for pure *n*-octacosane ($C_{28}H_{58}$) wax crystals prepared in the absence of any copolymer additive at 20 °C as (a) a 5.0% w/w suspension in *n*-dodecane using bright field optical microscopy, and (b) dried crystals examined by SEM. (c) Normalized transmittance (%) at λ = 650 nm *vs.* temperature plot for 5.0% w/w solutions of *n*-octacosane in *n*-dodecane on cooling from 50 °C to 0 °C (blue open triangles) and on heating from 0 °C to 50 °C (orange solid circles) at a cooling/heating rate of 1.0 °C min^{-1}. The temperatures required for zero transmittance on cooling (T_{cool}) and 100% transmittance on heating (T_{heat}) are labeled. Digital photographs show the formation of a transparent solution at 50 °C and the same sample becoming opaque after cooling to 0 °C.

temperature required for 0% transmittance on cooling (*i.e.* the temperature at which crystallization is judged to be complete). T_{cool} occurred at around 19 °C, which is typically a few degrees

Table 2 Composition of (co)polymer additive and mean T_{cool} for wax-(co)polymer mixtures as determined by turbidimetry studies. Wax-(co)polymer mixtures contain 5.0% w/w $C_{28}H_{58}$ in *n*-dodecane with 0.26 mM (co)polymer additive

(Co)polymer composition	T_{cool} wax + (co)polymer[a]/°C
—	19.3 ± 0.5
L_{98}	16.8 ± 0.1
Be_{37}	18.9 ± 0.1
L_{98}-*b*-Be_{10}	15.7 ± 0.1
L_{98}-*b*-Be_{20}	15.6 ± 0.1
L_{98}-*b*-Be_{40}	14.1 ± 0.5
L_{98}-*b*-Be_{60}	14.7 ± 0.1
L_{100}-*stat*-Be_{10}	15.0 ± 0.1
L_{100}-*stat*-Be_{20}	16.2 ± 0.5
L_{100}-*stat*-Be_{40}	13.7 ± 1.2
L_{100}-*stat*-Be_{60}	14.0 ± 0.5

[a] Mean values and corresponding standard deviations calculated from turbidimetry studies conducted for three consecutive heating/cooling cycles.

below the WAT. The former parameter was used to compare various wax-copolymer mixtures as it can be readily identified from transmittance *vs.* temperature plots. On reheating to 50 °C, a transparent solution (100% transmittance) was obtained. The minimum temperature corresponding to 100% transmittance on heating is denoted as T_{heat}. As anticipated for a first-order phase transition, some thermal hysteresis is observed, *i.e.* the sharp increase in transmittance on heating occurs approximately 10 °C higher than the corresponding reduction in transmittance during cooling. This is attributed to a kinetic energy barrier associated with the formation of wax crystals on cooling, whereas the corresponding melting event involves no such barrier. Similar hysteretic behavior has been reported in the literature.[37,40]

Turbidimetry data obtained for a series of eleven experiments conducted using 5.0% w/w *n*-octacosane in *n*-dodecane in the absence or presence of BeMA-based copolymers at a fixed molar concentration of 0.26 mM are presented in Table 2. Each T_{cool} value and corresponding standard deviation was calculated from three consecutive heating/cooling cycles. In all cases, the T_{cool} value was a few degrees below the WAT. The *n*-octacosane wax in *n*-dodecane exhibited a T_{cool} of 19.3 ± 0.5 °C in the absence of any (co)polymer. This T_{cool} value remained unchanged (within experimental error) in the presence of the $PBeMA_{37}$ homopolymer. In contrast, addition of $PLMA_{98}$ homopolymer reduced T_{cool} to 16.8 ± 0.1 °C. However, the greatest reduction in T_{cool} was achieved by using BeMA-based diblock or statistical copolymers, with the copolymer

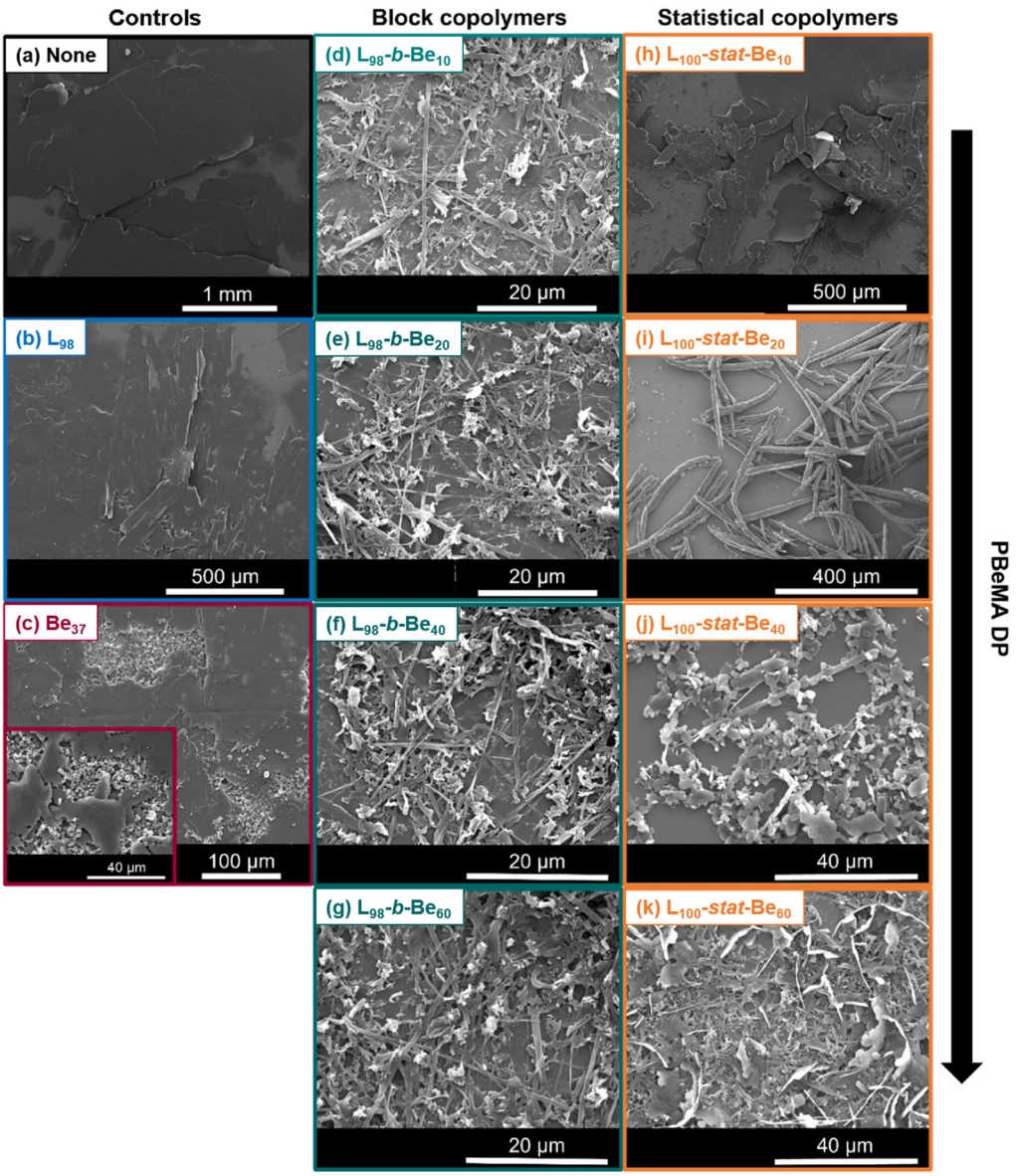

Fig. 5 SEM images recorded for wax crystals formed by cooling solutions of 5.0% w/w *n*-octacosane in *n*-dodecane in the absence or presence of various (co)polymers at a constant (co)polymer concentration of 0.26 mM.

architecture making surprisingly little difference. BeMA-rich diblock or statistical copolymers reduce T_{cool} by approximately 5 °C compared to that observed for the pure wax in *n*-dodecane in the absence of any copolymer. Other workers have previously reported similar observations for effective wax crystal modifiers.[33–35] For instance, Sjöblom *et al.* reported WAT reductions between 1.4 and 5.5 °C for 5.0% w/w macrocrystalline wax in toluene in the presence of various commercial and putative PPDs.[25] It is generally accepted that polymers reduce the WAT of a wax by changing its solubility equilibrium.[6,25,27,36] Polymers interact with (or become incorporated into) the precipitating wax crystals, which in turn results in slower dissolution kinetics.[35]

It is well-established that wax inhibitors and PPDs can alter the morphology of wax crystals.[6] Such polymeric additives are believed to delay nucleation, and either adsorb onto or co-crystallize with paraffin waxes.[12,48] To ensure the same heating/cooling rate for all the wax-copolymer mixtures, optical microscopy and SEM images were always acquired after performing turbidimetry measurements at a heating/cooling rate of 1.0 °C min^{-1}. After the third cooling sweep from 50 °C to 0 °C, each sample was returned to 20 °C at a heating rate of 1.0 °C min^{-1}. Turbidimetry studies confirmed that 20 °C is a sufficiently low temperature to maintain crystals (*i.e.* just below T_{heat} for the wax-copolymer mixtures). Optical microscopy was employed to determine the wax crystal size and morphology in solution, while SEM images were recorded for the dried wax crystals. The former technique showed that wax crystals were formed as large clumps of platelets (mean length, $l \approx 0.5$–2.5 mm) when cooling a 5.0% w/w solution of *n*-octacosane in *n*-dodecane from 50 °C to 0 °C (Fig. 4b). Large platelets, up to 2 mm in length, are also discernible in SEM images obtained for dried *n*-octacosane wax crystals (Fig. 5a). Binks and co-workers reported the formation of similar irregularly-shaped thin platelets when cooling solutions of either a $C_{24}H_{50}$ wax in toluene or a $C_{36}H_{74}$ wax in heptane in the absence of any copolymer additive.[37] Fetters and co-workers reported a 3D 'house of cards' structure when using optical microscopy to characterize wax crystals on cooling a 4% w/w solution of similar *n*-paraffins in *n*-decane to 0 °C.[8,14]

The effect of using a fixed copolymer concentration of 0.26 mM on the wax crystal size and morphology was further studied by SEM (Fig. 5). Addition of a $PLMA_{98}$ homopolymer had minimal effect on the size and morphology of the *n*-octacosane crystals (Fig. 5b). More specifically, large, irregular platelets were observed that resembled those obtained for the pure wax shown in Fig. 5a. Similar platelets were also observed for wax crystals prepared in the presence of a $PBeMA_{37}$ homopolymer (Fig. 5c), but small clumps of approximately 5 μm diameter were also visible. Interestingly, addition of a $PLMA_{98}$-$PBeMA_x$ diblock copolymer resulted in significantly smaller wax crystals. All four diblock copolymer compositions examined (*i.e.* x = 10, 20, 40 or 60) produced similar crystal morphologies; a mixture of irregular-shaped clumps (~2–10 μm) and needle-like crystals [length, $l = 25 \pm 17$ μm (averaged over 175 crystals); width, $w = 0.7 \pm 0.3$ μm (averaged over 50 crystals); mean aspect ratio, l/w = 31] are represented in Fig. 5d–g. There are many literature examples of polymeric wax crystal modifiers producing relatively small wax crystals.[19,25–29] This is useful because it can improve crude oil flowability. Fewer

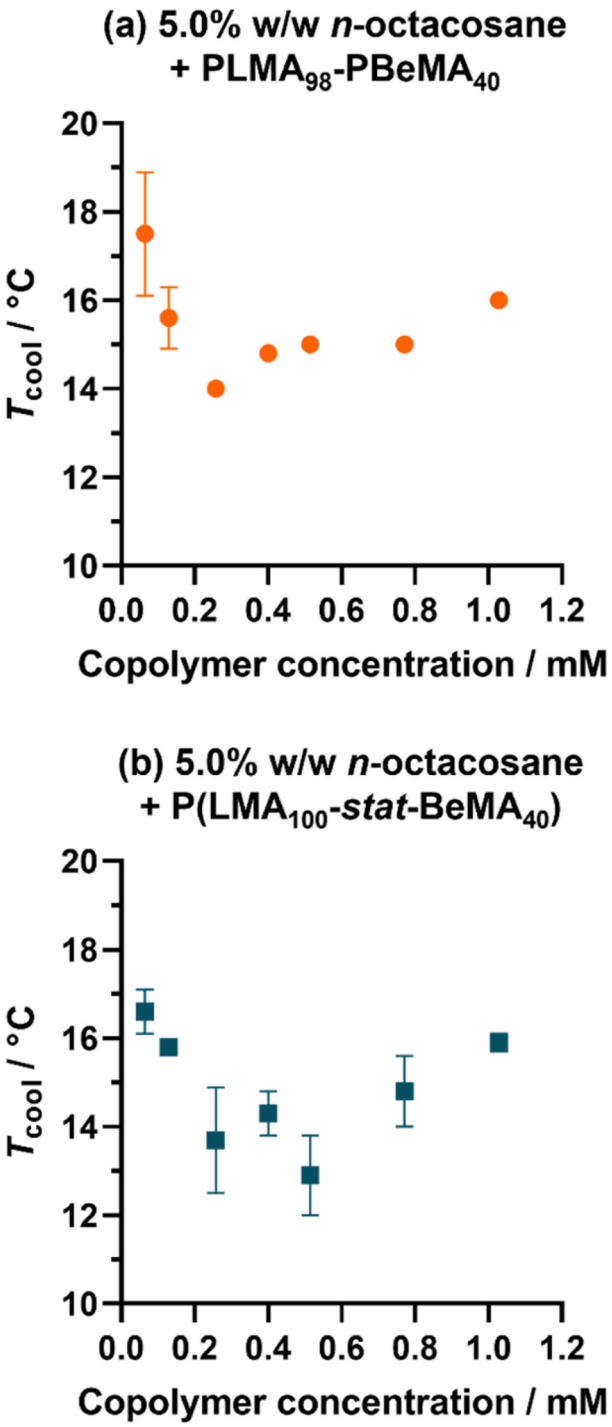

Fig. 6 T_{cool} *vs.* copolymer concentration plots for 5.0% w/w *n*-octacosane in *n*-dodecane for (a) $PLMA_{98}$-$PBeMA_{40}$ diblock copolymer, and (b) $P(LMA_{100}$-*stat*-$BeMA_{40})$ statistical copolymer. Error bars indicate the standard deviation from three repeat measurements. Such error bars lie within the data points in some cases.

contacts between neighboring crystals lead to weaker gel networks, so the removal of waxy deposits becomes easier.[7,28] In principle, increasing the anisotropy of wax crystals to produce elongated needle-like structures should also reduce gel strength relative to that for the 'house of cards' networks formed by large platelets.[8,49]

In contrast to the four $PLMA_{98}$-$PBeMA_x$ diblock copolymers, the BeMA content of the four P(LMA_{100}-*stat*-$BeMA_x$) statistical copolymers had a discernible effect on their wax crystal modifier performance. Thus, using the P(LMA_{100}-*stat*-$BeMA_{10}$) statistical copolymer mainly resulted in the formation of large platelets (Fig. 5h), although some smaller (<200 μm) and more elongated crystals were also present. However, a strikingly different wax crystal morphology was obtained when using P(LMA_{100}-*stat*-$BeMA_{20}$): large needle-like crystals [l = 280 ± 136 μm (averaged over 80 crystals); w = 13 ± 3 μm (averaged over 50 crystals); l/w = 22] were observed almost exclusively (Fig. 5i). Fetters and co-workers observed a similar crystal morphology when investigating the influence of semi-crystalline poly(ethylene-*stat*-butene) (PEB) statistical copolymers on the crystallization of *n*-octacosane.[14] On cooling this model wax (4% w/w in *n*-decane) to 0 °C in the presence of 0.05–0.3% w/w PEB7.5, crystals described as 'long sticks' ($l \approx$ 50–100 μm) were observed by optical microscopy. According to Bai and Zhang, such rod-like crystals provide fewer opportunities for inter-particle interactions than platelets, resulting in significantly weaker crystal–crystal interactions.[49]

Increasing the mean number of PBeMA repeat units per copolymer chain up to 40 or 60 resulted in much smaller crystals. In particular, mixtures of small platelets ($l \approx$ 5–10 μm) and a few needle-like crystals ($l \approx$ 50 μm) were observed in Fig. 5j and small platelets co-existing with smaller needle-like crystals can be observed in Fig. 5k. Fetters and co-workers also reported the formation of smaller *n*-octacosane wax crystals ('short bars') in the presence of a higher PEB concentration (0.85 w/w), as opposed to the 'long sticks' that were formed at lower copolymer concentrations.[14]

In summary, the presence of various PBeMA-based diblock or statistical copolymers at a fixed copolymer concentration of 0.26 mM influenced the morphology of the wax crystals formed when cooling a 5.0% w/w solution of *n*-octacosane in *n*-dodecane. In some cases, a significant reduction in the overall crystal dimensions and/or an increase in the crystal aspect ratio was observed. For the diblock copolymers, increasing the mean DP of PBeMA had a relatively weak effect on the wax crystal morphology. Smaller wax crystals (<50 μm) were observed by SEM for all four diblock copolymers. In striking contrast, large needle-like crystals were obtained when increas-

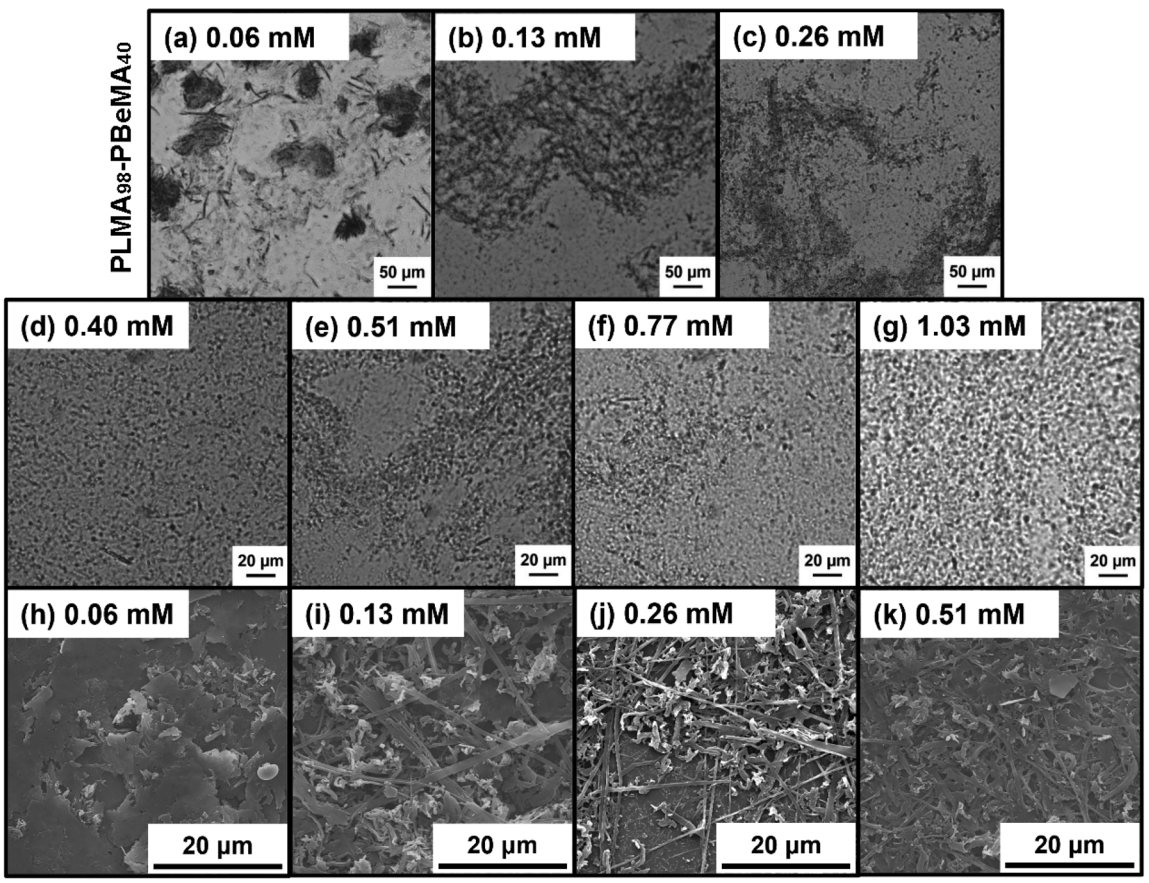

Fig. 7 Representative images of wax crystals formed on cooling 5.0% w/w *n*-octacosane in *n*-dodecane in the presence of $PLMA_{98}$-$PBeMA_{40}$ at various copolymer concentrations obtained by (a)–(g) optical microscopy, and (h)–(k) SEM.

ing the BeMA content of the statistical copolymers from 10 to 20 repeat units per copolymer chain, while relatively small wax crystals were formed at 40 BeMA repeat units per copolymer chain. Yao *et al.* demonstrated that the addition of EVA resulted in a reduction in the wax precipitation temperature and concluded that co-crystallization was the dominant wax-copolymer interaction.[50] The dominant interaction mechanism for the copolymers studied herein is also likely to be co-crystallization of the pendent behenyl groups with the *n*-octacosane wax crystals. This interpretation is supported by the reduction in T_{cool} indicated by turbidimetry studies.

The effect of varying the total molar concentration of the copolymers on (i) the T_{cool} values identified by turbidimetry studies and (ii) the wax crystal morphology was investigated for selected copolymers. In particular, $PLMA_{98}$-$PBeMA_{40}$ and $P(LMA_{100}$-*stat*-$BeMA_{40})$ were chosen to compare the diblock and statistical copolymer architecture because this pair produced the lowest T_{cool} values as judged by turbidimetry, as well as some of the smallest crystals when employed at a fixed copolymer concentration (0.26 mM). The copolymer concentration was systematically varied from 0.06 to 1.03 mM and turbidimetry studies were used to identify T_{cool} for wax-copolymer mixtures in each case. For 5.0% w/w *n*-octacosane in *n*-dodecane, T_{cool} was reduced from 17.5 °C to 14.0 °C when increasing the $PLMA_{98}$-$PBeMA_{40}$ concentration from 0.06 to 0.26 mM (Fig. 6a). However, higher concentrations produced an increase in T_{cool} up to 16.0 °C. A similar concentration dependence was also observed for $P(LMA_{100}$-*stat*-$BeMA_{40})$: a minimum T_{cool} value of 12.9 °C was measured at a copolymer concentration of 0.51 mM (Fig. 6b). Such behavior suggests two competing effects, but it is not clear why the initial interaction between the copolymer chains and the wax crystals should be reduced at higher copolymer concentrations.

Moreover, the *n*-octacosane crystals obtained in the presence of the $PLMA_{98}$-$PBeMA_{40}$ diblock copolymer were imaged at 20 °C by optical microscopy (Fig. 7). Larger wax crystals were formed at lower copolymer concentrations (≤0.26 mM), with a mixture of irregular-shaped and needle-like crystals being observed in Fig. 7a–c. The smaller crystals observed above 0.26 mM (Fig. 7d–g) were also examined by SEM to obtain higher resolution images (Fig. 7h–k). Fig. 7h shows platelets prepared at a copolymer concentration of 0.06 mM, while mixtures of irregular-shaped and needle-like crystals obtained at copolymer concentrations of 0.13 mM, 0.26 mM and 0.51 mM are shown in Fig. 7i–k.

A series of *n*-octacosane crystals formed in the presence of $P(LMA_{100}$-*stat*-$BeMA_{40})$ were imaged in solution at 20 °C by optical microscopy and after drying by SEM (Fig. 8). Large

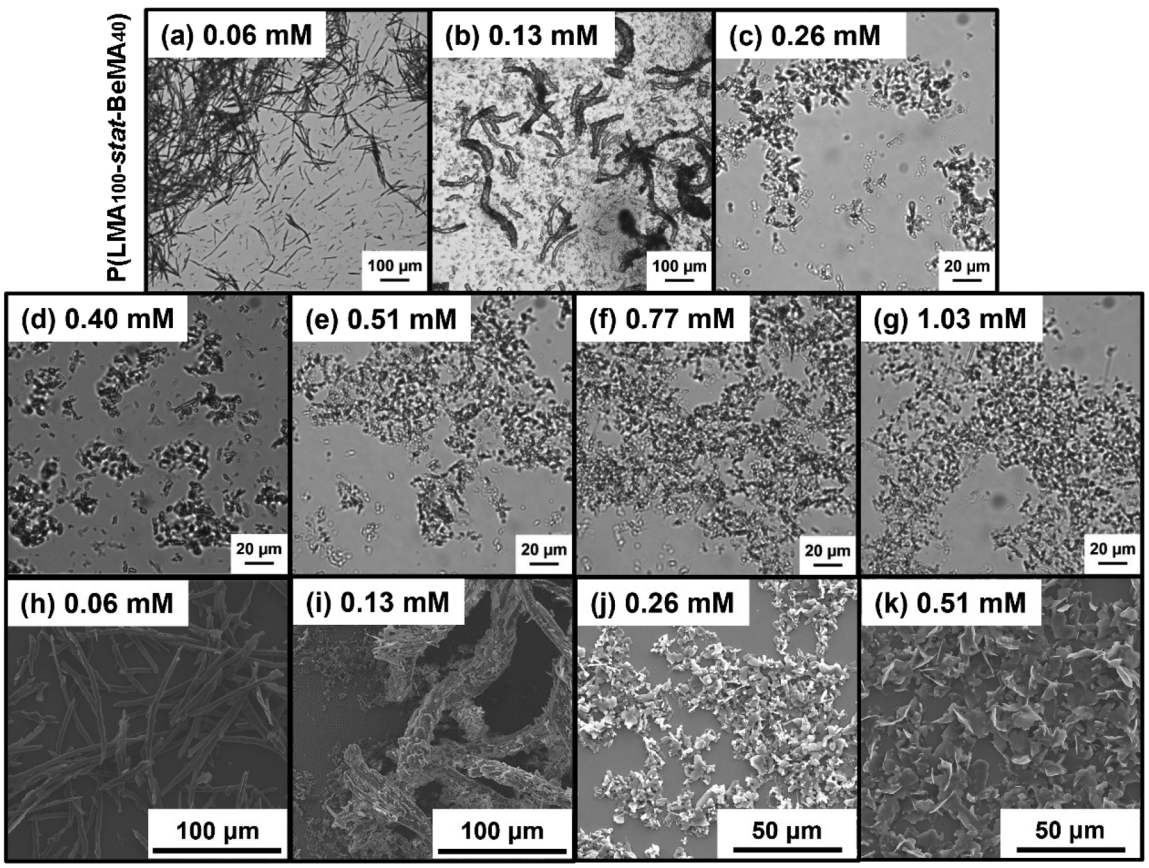

Fig. 8 Representative images of wax crystals formed on cooling 5.0% w/w *n*-octacosane in *n*-dodecane in the presence of $P(LMA_{100}$-*stat*-$BeMA_{40})$ at various copolymer concentrations obtained by (a)–(g) optical microscopy, and (h)–(k) SEM.

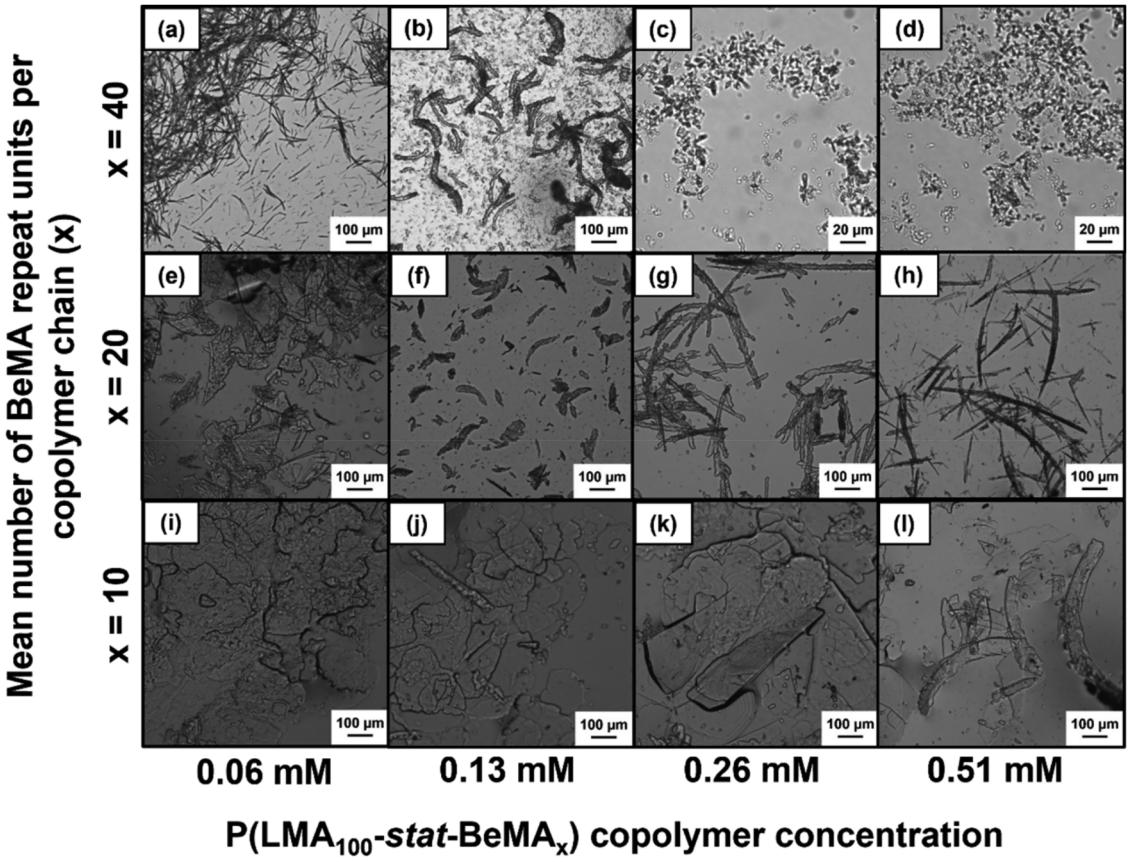

Fig. 9 Optical microscopy images obtained for wax crystals formed by a 5.0% w/w dispersion of *n*-octacosane in *n*-dodecane in the presence of various concentrations of P(LMA_{100}-*stat*-$BeMA_x$), where x = 10, 20 or 40.

needle-like structures [l = 77 ± 28 μm (averaged over 50 crystals); w = 3.3 ± 0.8 μm (averaged over 50 crystals); mean aspect ratio, l/w = 23] were obtained at a copolymer concentration of 0.06 mM (Fig. 8a and h). These wax crystals were smaller, but their mean aspect ratio was comparable to that of the needles formed in the presence of P(LMA_{100}-*stat*-$BeMA_{20}$) at 0.26 mM (Fig. 5i). Large, relatively thick needles ($l \approx$ 100–300 μm; $w \approx$ 10–20 μm) containing a secondary population of notably smaller crystals were obtained at 0.13 mM (Fig. 8b and i). For copolymer concentrations at or above 0.26 mM, irregular-shaped wax crystals of less than 50 μm were observed by both optical microscopy and SEM, as shown in Fig. 8c–g, j and k, respectively.

A morphology map based on optical microscopy images (Fig. 9) was used to illustrate the effect of varying copolymer composition and concentration on the wax crystal morphology when using P(LMA_{100}-*stat*-$BeMA_x$). For the copolymer with the lowest BeMA content, relatively large crystals were formed at all copolymer concentrations. For P(LMA_{100}-*stat*-$BeMA_{20}$), the large platelets produced at a copolymer concentration of 0.06 mM are replaced by needle-like crystals at higher copolymer concentrations. For the copolymer with the highest BeMA content, relatively fine needles are produced at 0.06 mM, with much smaller, irregular crystals being formed at higher copolymer concentrations. These observations suggest that statistical copolymers with higher BeMA contents (*i.e.*, x = 50 or 60) may promote the formation of relatively small crystals at copolymer concentrations at or below 0.06 mM. This conjecture warrants further studies.

Conclusions

In summary, two series of $PLMA_{98}$-$PBeMA_x$ diblock and P(LMA_{100}-*stat*-$BeMA_x$) statistical copolymers were prepared *via* RAFT solution polymerization at 80% w/w solids in *n*-dodecane. High monomer conversions (≥98%) and relatively narrow molecular weight distributions ($Đ \leq 1.25$) were obtained for all copolymers. DSC studies confirmed that the P(LMA_{100}-*stat*-$BeMA_x$) statistical copolymers exhibited significantly lower crystallization and melting temperatures than $PLMA_{98}$-$PBeMA_x$ diblock copolymers of almost identical overall composition.

All eight copolymers were evaluated as potential wax crystal modifiers for a 5.0% w/w dispersion of a model *n*-octacosane wax in *n*-dodecane, with $PLMA_{98}$ and $PBeMA_{37}$ homopolymers also being examined as reference materials. Temperature-dependent turbidimetry studies were conducted to determine

the wax crystallization temperature (or T_{cool}), which is the temperature at which zero transmittance is first recorded owing to wax crystallization. Typically, T_{cool} was a few degrees below the wax appearance temperature (WAT). At a constant molar copolymer concentration of 0.26 mM, there was negligible difference between the T_{cool} values obtained by turbidimetry studies for the various wax-copolymer mixtures. Each of the eight copolymers produced a reduction in T_{cool} of approximately 3–5 °C, with similar observations reported in the literature for effective wax crystal modifiers.[33–35]

SEM studies confirmed that the presence of such copolymers led to significant changes in the morphology of the wax crystals. Using either diblock or statistical copolymers at 0.26 mM produced a reduction in the overall size and/or an increase in the crystal aspect ratio. In principle, smaller crystals should improve the flow properties of crude oil because the wax crystals have a lower propensity to interact with each other and therefore form weaker gels.[7,25,28] In addition, for the $PLMA_{98}$-$PBeMA_x$ diblock copolymer series, increasing the mean PBeMA DP from 10 to 60 had surprisingly little effect on the wax crystal morphology. Relatively small crystals of less than 50 μm were observed by SEM for all four diblock copolymers. In contrast, strikingly different needle-like crystals are obtained simply by increasing the BeMA content of the P(LMA_{100}-*stat*-$BeMA_x$) statistical copolymers. Furthermore, for this copolymer series, increasing either the copolymer concentration or the mean number of BeMA repeat units per copolymer chain (x) led to the elongation of the initial platelets and the formation of needle-like structures, with subsequent formation of relatively small, irregular-shaped crystals. These observations suggest that statistical copolymers with higher BeMA contents could promote the formation of small crystals at copolymer concentrations at or below 0.06 mM.

The dominant interaction mechanism for such copolymers appears to be co-crystallization of the wax with the pendent behenyl chains in the PBeMA units, thus altering the size and shape of the growing wax crystals. This is supported by the reduction in T_{cool} for a 5.0% w/w wax dispersion in *n*-dodecane in the presence of such copolymers, as indicated by turbidimetry studies. Overall, the BeMA-based diblock and statistical copolymers studied herein are interesting new wax crystal modifiers. However, the statistical copolymers may offer an advantage over their diblock counterparts, as they are easier to prepare and do not suffer from any homopolymer contamination.

Conflicts of interest

There are no conflicts to declare.

Acknowledgements

EPSRC is acknowledged for a Centre for Doctoral Training (CDT) grant that funded a PhD studentship for I. R. D. (EP/L016281).Scott Bader Ltd is thanked for partial support of this CDT PhD studentship and for permission to publish this work. S. P. A. acknowledges an EPSRC Particle Technology Established Career Fellowship grant (EP/R003009/1).

References

1 C. Chang, Q. D. Nguyen and H. P. Rønningsen, *J. Non-Newton. Fluid Mech.*, 1999, **87**, 127–154.
2 P. Singh, R. Venkatesan, H. S. Fogler and N. Nagarajan, *AIChE J.*, 2000, **46**, 1059–1074.
3 H. P. Roenningsen, B. Bjoerndal, A. B. Hansen and W. B. Pedersen, *Energy Fuels*, 1991, **5**, 895–908.
4 A. M. Al-Sabagh, M. R. Noor El-Din, R. E. Morsi and M. Z. Elsabee, *J. Pet. Sci. Eng.*, 2009, **65**, 139–146.
5 Y. Wu, G. Ni, F. Yang, C. Li and G. Dong, *Energy Fuels*, 2012, **26**, 995–1001.
6 Y. Chi, J. Yang, C. Sarica and N. Daraboina, *Energy Fuels*, 2019, **33**, 2797–2809.
7 M. Senra, T. Scholand, C. Maxey and H. S. Fogler, *Energy Fuels*, 2009, **23**, 5947–5957.
8 H. S. Ashbaugh, A. Radulescu, R. K. Prud'homme, D. Schwahn, D. Richter and L. J. Fetters, *Macromolecules*, 2002, **35**, 7044–7053.
9 G. A. Holder and J. Winkler, *J. Inst. Pet.*, 1965, **51**, 235–242.
10 P. Singh, H. S. Fogler and N. Nagarajan, *J. Rheol.*, 1999, **43**, 1437–1459.
11 R. Venkatesan, P. Singh and H. S. Fogler, *Soc. Pet. Eng. J.*, 2002, **7**, 349–352.
12 F. Yang, Y. Zhao, J. Sjöblom, C. Li and K. G. Paso, *J. Dispersion Sci. Technol.*, 2015, **36**, 213–225.
13 D. Schwahn, D. Richter, M. Lin and L. J. Fetters, *Macromolecules*, 2002, **35**, 3762–3768.
14 X. Guo, B. A. Pethica, J. S. Huang, R. K. Prud'homme, D. H. Adamson and L. J. Fetters, *Energy Fuels*, 2004, **18**, 930–937.
15 A. Radulescu, D. Schwahn, J. Stellbrink, E. Kentzinger, M. Heiderich, D. Richter and L. J. Fetters, *Macromolecules*, 2006, **39**, 6142–6151.
16 W. Leube, M. Monkenbusch, D. Schneiders, D. Richter, D. Adamson, L. Fetters, P. Dounis and R. Lovegrove, *Energy Fuels*, 2000, **14**, 419–430.
17 H. S. Ashbaugh, L. J. Fetters, D. H. Adamson and R. K. Prud'homme, *J. Rheol.*, 2002, **46**, 763–776.
18 A. L. Machado, E. F. Lucas and G. González, *J. Pet. Sci. Eng.*, 2001, **32**, 159–165.
19 H. S. Ashbaugh, X. Guo, D. Schwahn, R. K. Prud'homme, D. Richter and L. J. Fetters, *Energy Fuels*, 2005, **19**, 138–144.
20 E. Marie, Y. Chevalier, F. Eydoux, L. Germanaud and P. Flores, *J. Colloid Interface Sci.*, 2005, **290**, 406–418.
21 J. B. Taraneh, G. Rahmatollah, A. Hassan and D. Alireza, *Fuel Process. Technol.*, 2008, **89**, 973–977.
22 R. A. Soldi, A. R. S. Oliveira, R. V. Barbosa and M. A. F. César-Oliveira, *Eur. Polym. J.*, 2007, **43**, 3671–3678.
23 Y. Song, S. Han and T. Ren, *Pet. Sci. Technol.*, 2010, **28**, 860–867.

24 G. Moriceau, D. Lester, G. S. Pappas, P. O'Hora, J. Winn, T. Smith and S. Perrier, *Energy Fuels*, 2019, **33**, 7257–7264.
25 J. Ruwoldt, S. Simon, J. Norrman, H. J. Oschmann and J. Sjöblom, *Energy Fuels*, 2017, **31**, 6838–6847.
26 K. Cao, Q. J. Zhu, X. X. Wei and Z. Yao, *Energy Fuels*, 2015, **29**, 993–1000.
27 K. G. Paso, K. K. Krückert, H. J. Oschmann, H. Ali and J. Sjöblom, *J. Pet. Sci. Eng.*, 2014, **115**, 38–49.
28 H. R. Jafari Ansaroudi, M. Vafaie-Sefti, S. Masoudi, T. J. Behbahani and H. Jafari, *Pet. Sci. Technol.*, 2013, **31**, 643–651.
29 X. Guo, B. A. Pethica, J. S. Huang, D. H. Adamson and R. K. Prud'homme, *Energy Fuels*, 2006, **20**, 250–256.
30 K. S. Pedersen and H. P. Rønningsen, *Energy Fuels*, 2003, **17**, 321–328.
31 L. Fang, X. Zhang, J. Ma and B. Zhang, *Ind. Eng. Chem. Res.*, 2012, **51**, 11605–11612.
32 B. Coto, C. Martos, J. J. Espada, M. D. Robustillo and J. L. Peña, *Energy Sci. Eng.*, 2014, **2**, 196–203.
33 T. Wang, J. Xu, M. Wang, X. Wei, M. Shen, J. Huang, R. Zhang, L. Li and X. Guo, *J. Appl. Polym. Sci.*, 2015, **132**, 41660.
34 J. Xu, H. Jiang, T. Li, X. Wei, T. Wang, J. Huang, W. Wang, A. L. Smith, J. Wang, R. Zhang, Y. Xu, L. Li, R. K. Prud'Homme and X. Guo, *Ind. Eng. Chem. Res.*, 2015, **54**, 5204–5212.
35 K.-S. Wang, C.-H. Wu, J. L. Creek, P. J. Shuler and Y. Tang, *Pet. Sci. Technol.*, 2003, **21**, 359–368.
36 P. Claudy, J. M. Létoffé, B. Bonardi, D. Vassilakis and B. Damin, *Fuel*, 1993, **72**, 821–827.
37 B. P. Binks, P. D. I. Fletcher, N. A. Roberts, J. Dunkerley, H. Greenfield, A. Mastrangelo and K. Trickett, *Phys. Chem. Chem. Phys.*, 2015, **17**, 4107–4117.
38 P. Cacioli, D. G. Hawthorne, R. L. Laslett, E. Rizzardo and D. H. Solomon, *J. Macromol. Sci. A*, 1986, **23**, 839–852.
39 M. Rodlert, E. Harth, I. Rees and C. J. Hawker, *J. Polym. Sci., Part A: Polym. Chem.*, 2000, **38**, 4749–4763.
40 M. J. Derry, O. O. Mykhaylyk, A. J. Ryan and S. P. Armes, *Chem. Sci.*, 2018, **9**, 4071–4082.
41 F. Fleischhaker, A. P. Haehnel, A. M. Misske, M. Blanchot, S. Haremza and C. Barner-Kowollik, *Macromol. Chem. Phys.*, 2014, **215**, 1192–1200.
42 M. Semsarilar, N. J. W. Penfold, E. R. Jones and S. P. Armes, *Polym. Chem.*, 2015, **6**, 1751–1757.
43 U. N. Arua and F. D. Blum, *J. Polym. Sci. B: Polym. Phys.*, 2018, **56**, 89–96.
44 S. S. Rogers and L. Mandelkern, *J. Phys. Chem.*, 1957, **61**, 985–990.
45 H. A. Schneider, *Polymer*, 2005, **46**, 2230–2237.
46 M. Kurniawan, J. Ruwoldt, J. Norrman and K. G. Paso, *Energy Fuels*, 2021, **35**, 7666–7680.
47 J. Jennings, M. F. Butler, M. McLeod, E. Csányi, A. J. Ryan and O. O. Mykhaylyk, *Cryst. Growth Des.*, 2018, **18**, 7094–7105.
48 Y. H. Jang, M. Blanco, J. Creek, Y. Tang and W. A. Goddard, *J. Phys. Chem. B*, 2007, **111**, 13173–13179.
49 C. Bai and J. Zhang, *Ind. Eng. Chem. Res.*, 2013, **52**, 2732–2739.
50 B. Yao, C. Li, F. Yang, X. Zhang, Z. Mu, G. Sun and Y. Zhao, *Energy Fuels*, 2018, **32**, 1567–1578.